JMEPEG
https://doi.org/10.1007/s11665-024-09657-3

1059-9495/$19.00

ORIGINAL RESEARCH ARTICLE

Comparison of Mechanical Properties of Bulk NiAl-Re-Al_2O_3 Intermetallic Material Manufactured by Laser Powder Bed Fusion and Hot Pressing

Kamil Bochenek, Siegfried Arneitz, Christof Sommitsch, and Michał Basista

Submitted: 15 November 2023 / Revised: 20 April 2024 / Accepted: 26 April 2024

The low fracture toughness of NiAl at room temperature is one of the critical issues limiting its application in aircraft engines. It has been previously shown that a small addition of rhenium and alumina significantly improves the fracture toughness of hot-pressed NiAl. In this work, NiAl with an admixture of rhenium and alumina was produced by laser powder bed fusion additive technology (LPBF). The purpose was to compare the fracture toughness, bending strength, and microhardness of the NiAl-Re-Al_2O_3 material produced by LPBF and hot pressing (HP). Our results show that the LPBF material has lower fracture toughness and bending strength compared to its hot-pressed equivalent. Microcracks generated by thermal stresses during the LPBF process were the primary cause of this behavior. To improve the LPBF material, a post-processing by HP was applied. However, the fracture toughness of the (LPBF + HP) material remained at 50% of the K_{IC} of the HP material. This study supports hot pressing as a suitable processing method for NiAl with rhenium and alumina additions. However, a hybrid approach combining LPBF and HP proved to be highly effective on the raw NiAl powder, resulting in superior fracture toughness of the final material compared to that consolidated by singular HP.

Keywords NiAl intermetallic, additive manufacturing, hot pressing, mechanical properties

1. Introduction

Among many advanced materials for high-temperature applications in the aerospace industry, nickel aluminide (NiAl) has attracted the attention of both science and industry as a possible replacement for nickel superalloys. High melting point, low density, high thermal conductivity, thermal stability, and high oxidation resistance are the major advantages of NiAl. However, low fracture toughness and insufficient ductility at room temperature restricted the application of NiAl, especially in high-pressure turbine blades and vanes. For almost half a century, NiAl has been a topic of intensive research, but the above drawbacks have not been overcome yet, and solutions are still being sought by modifying the NiAl morphology and using different processing techniques (see the review papers (Ref 1-4)).

From a wide spectrum of processing methods available for intermetallics, casting is most commonly used to fabricate bulk NiAl-based alloys (Ref 5-8). An improvement of the room-temperature mechanical properties of NiAl, particularly the fracture toughness (K_{IC}), can also be obtained via a combined effect of rhenium and aluminum oxide addition to NiAl powder consolidated by hot pressing (HP) as shown in our previous works (Ref 9, 10). The main aim of the present work is to extend the previous investigations on NiAl modified with Re and Al_2O_3 by employing one of the widely used additive manufacturing techniques, namely that of laser powder bed fusion (LPBF).

The refractory transition metals such as vanadium, chromium, molybdenum (Ref 11-13) form a quasi-binary eutectic system, which according to simulations and theoretical calculations (Ref 14-16), can promote the activation of an additional slip system in NiAl which in turn can improve fracture toughness. The above systems with V, Cr, and Mo have been widely studied in research papers for more than three decades. The effect of increasing the fracture toughness of NiAl can also be achieved with another transition metal, rhenium. However, only a few papers have addressed the influence of rhenium on the NiAl system (Ref 13, 17-19). We have shown in our previous work (Ref 9) that the addition of 1.53 vol% of rhenium to NiAl, which corresponds to the eutectic composition of the NiAl-Re system determined by Rablbauer et al. (Ref 19), and sintering of the NiAl + 1.53 vol%Re by conventional HP results in an improvement in fracture toughness from 8.08 MPa $\sqrt{m}$ for pure NiAl to 12.61 MPa $\sqrt{m}$ for NiAl + 1.53 vol%Re.

Further research to improve the fracture toughness of NiAl at room temperature (Ref 10) consisted of adding fine alumina particles and consolidating the NiAl/Re/Al_2O_3 powder mixture by hot pressing. Although it may seem counterintuitive to add alumina ceramics to the NiAl-Re system to increase its fracture toughness, this is not the case. As shown by Ur et al. (Ref 20), the ceramic grains distributed along the grain boundaries of NiAl can act as obstacles to dislocation motion and directly lead to the improvement of mechanical properties. In addition,

Kamil Bochenek and **Michał Basista**, Institute of Fundamental Technological Research, Polish Academy of Sciences, Pawińskiego 5B, 02-106, Warsaw, Poland; and **Siegfried Arneitz** and **Christof Sommitsch**, Institute of Materials Science, Joining and Forming, Graz University of Technology, Kopernikusgasse 24/I, 8010 Graz, Austria. Contact e-mail: kboch@ippt.pan.pl.

Published online: 04 June 2024

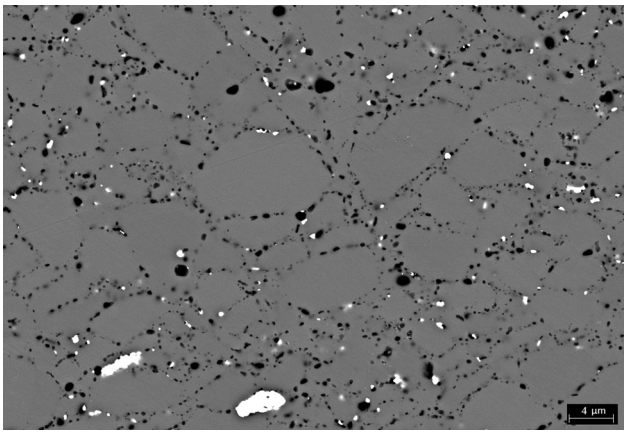

Fig. 1 SEM image of NiAl + 0.73Re + 0.5Al_2O_3 (vol%) composite consolidated by HP. White grains are rhenium, small black dots at NiAl grain boundaries represent *in situ* formed Al_2O_3 during ball milling in air, larger black dots are alumina grains from powder added during material processing. Reproduced from: K. Bochenek, W. Węglewski, J. Morgiel, M. Maj, and M. Basista, "Enhancement of fracture toughness of hot-pressed NiAl-Re material by aluminum oxide addition," *Mater. Sci. Eng. A*, vol 790, p. 139670, 2020, with permission from Elsevier

the presence of fine alumina grains at the grain boundaries can restrict grain growth, which also affects the mechanical properties (Ref 21). Inspired by these works, in Ref. (Ref 10) we investigated the effect of alumina addition on the fracture toughness of the NiAl + 1.53 vol%Re material developed in (Ref 9) with the aim to further improve its fracture toughness at RT. As a result of optimizing the material composition and process conditions, the NiAl + 0.73Re + 0.5Al_2O_3(vol%) composite was selected from all the material compositions analyzed in (Ref 10). The fracture toughness of NiAl + 0.73Re + 0.5 Al_2O_3(vol%) composite reached 15.19 MPa $\sqrt{m}$ as compared to 8.08 MPa $\sqrt{m}$ for pure NiAl sintered under the same conditions. Incidentally, this result was not obtained for the eutectic concentration of 1.53 vol% Re, but for 0.73 vol% Re, which is about half of the eutectic concentration of the NiAl-Re system determined in (Ref 19).

The SEM image of the NiAl + 0.73Re + 0.5Al_2O_3(vol%) composite in Fig. 1 shows two families of alumina grains (black dots) at the NiAl grain boundaries, which apparently contributed to the increase in fracture toughness via the above-mentioned mechanisms of inhibiting dislocation movement and grain size growth.

In this paper, we compare the fracture behavior of NiAl + 0.73Re + 0.5Al_2O_3 (vol%) material fabricated by HP with the same composition material produced by the LPBF additive manufacturing technique, also using pure NiAl sinter as the reference material. The comparison includes the two processing methods mentioned above, and a hybrid method that is a combination of both methods (HP + LPBF), where the material produced by LPBF is further consolidated by HP. To make the comparison meaningful, all of the processes presented are carried out with the commercial powders supplied by the same producers as in the previous investigations (Ref 9, 10). Also, the hot pressing in the combined LPBF + HP process is performed using the same equipment and the same process parameters as the HP performed in (Ref 9, 10). However, as described in Section 2, the milling conditions are modified due to the LPBF requirements.

The LPBF, which belongs to the powder bed fusion (PBF) techniques, allows the obtaining of near-net-shape elements with high dimensional precision. In this technique, a laser melts the material which solidifies rapidly, resulting in a complex, fine-grained microstructure with a uniform chemical composition (Ref 22, 23). The additive manufacturing (AM) techniques have become highly attractive for advanced materials processing, especially in aerospace applications, since they reduce the material waste that occurs during the machining of the cast parts. Recent studies have shown that 3D printing can successfully be applied to produce high-density TiAl intermetallic and its alloys (Ref 24-27). On the other hand, manufacturing bulk NiAl using 3D printing was a topic of only a few research papers so far (Ref 28-30).

The industrial interest in AM (additive manufacturing) processes is derived from the almost unlimited design possibilities and the reduction of the machining process (Ref 31). AM technologies can be very attractive for the production of NiAl-based materials compared to casting as they avoid time-consuming machining and damage to the final parts due to the high brittleness of NiAl at room temperature. However, reports show that the mechanical properties of AM parts may not have sufficient mechanical properties compared to conventional manufacturing routes such as casting or hot pressing (Ref 32-34). Combining both types of manufacturing techniques—additive manufacturing and thermomechanical processing (e.g., forging, hot isostatic pressing (HIP), etc.)—can provide synergistic benefits derived from both techniques (Ref 35-37). The main benefits reported are an increase in material density due to the removal of porosity/voids remaining after the printing process and a reduction in residual stresses (Ref 38, 39).

This paper addresses some specific research questions. First, are the mechanical properties of the NiAl + 0.73Re + 0.5Al_2O_3 (vol%) material produced by LPBF better than those of NiAl + 0.73Re + 0.5Al_2O_3 (vol%) produced by HP? Second, can a hybrid approach combining these two techniques, namely LPBF to additively produce NiAl + 0.73Re + 0.5Al_2O_3 (vol%) from the powder mixture and HP to further consolidate the material printed by LPBF, improve the mechanical properties of NiAl + 0.73Re + 0.5Al_2O_3 (vol%) produced by either technique?

The combined use of 3D printing and HIP sintering has been previously reported in (Ref 40) for the fabrication of $Ni_{42}Al_{51}Cr_3Mo_4$ pre-alloyed powder, without addressing the influence of both methods on pure nickel aluminide material. The use of uniaxial pressing as in conventional HP or SPS processes, where the limited shape options are the main disadvantage, may be sufficient for the manufacture of turbine blades and vanes, as reported by Voisin et al. (Ref 41). Since the room temperature fracture toughness is a critical property of NiAl (Ref 1-3), this work is limited to RT mechanical testing only.

2. Material and Methods

It has been shown in (Ref 10) that the addition of 0.73 vol% Re and 0.5 vol% Al_2O_3 to the NiAl powder consolidated by hot pressing results in the highest enhancement of fracture toughness, bending strength, and tensile strength as compared with the reference material (sintered pure NiAl). For the LPBF processes reported in this paper, a commercial spherical powder of NiAl (GoodFellow, 99.0 % purity) was used for printing the reference material (pure NiAl). The commercial powders of Re

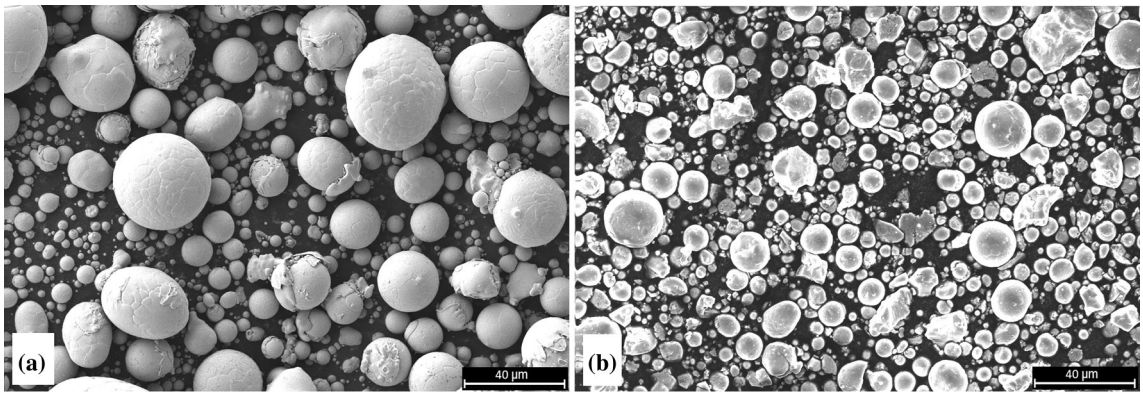

Fig. 2 SEM images of (a) NiAl raw powder and (b) NiAl + 0.73Re + 0.5Al_2O_3 powder mixture after 4 h of milling at 100 rpm

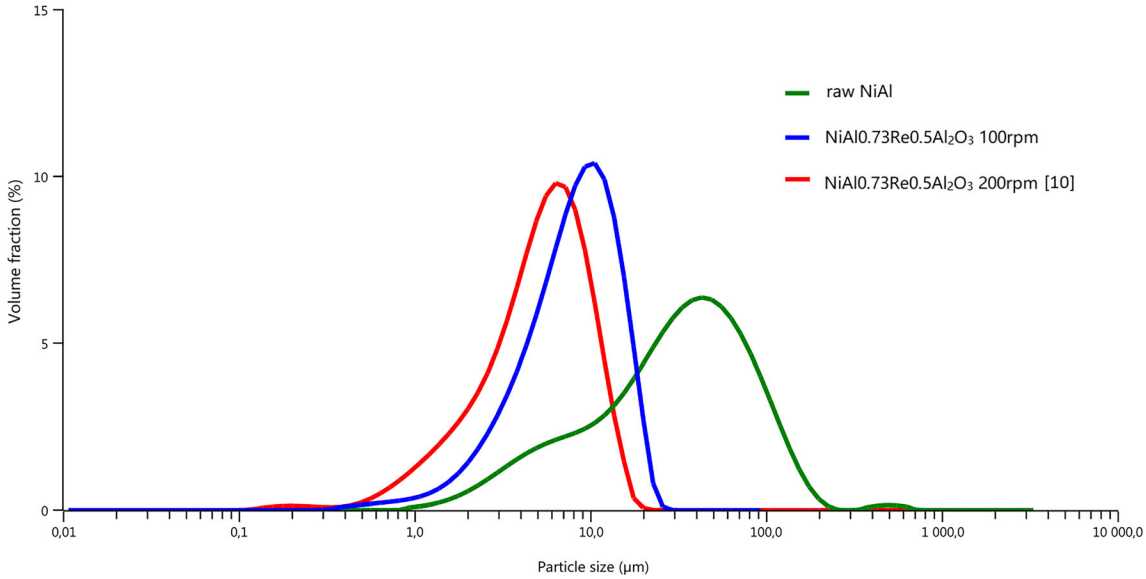

Fig. 3 Particle size distribution of raw NiAl, NiAl + 0.73Re + 0.5Al_2O_3 milled at 100 rpm, and NiAl + 0.73Re + 0.5Al_2O_3 milled at 200 rpm. The measured average particle size is 32.1, 8.1, and 5.3 μm, respectively

(99.7% purity) and Al_2O_3 (99.99% purity) were delivered by KGHM Polska Miedź and NewMetKoch, respectively. However, the milling procedure of NiAl with Re and Al_2O_3 additions described in (Ref 10) was not suitable for 3D printing technique used in this work due to high defragmentation and significant reduction of the average particle size of powder during the process. Therefore, to maintain the average particle size and ensure the sphericity of the NiAl powder after the mixing/milling process, a reduction of the rotational speed from 200 to 100 rpm was necessary. The NiAl + Re + Al_2O_3 powder feedstock for the LPBF process was prepared in a Fritsch Pulverisette 5 planetary ball mill. The following milling conditions were applied: rotational speed of 100 rpm, ball to powder weight ratio BPR 5:1, 20 min break after each 10 min of milling, and 4 h of the overall time of milling. In the following, the notation NiAl + 0.73Re + 0.5Al_2O_3 (vol%) used in the introduction will be reduced to NiAl + 0.73Re + 0.5Re, since only the volume fraction is used in the text. Figure 2(a) shows as-received NiAl powder used to prepare the reference material, whereas the morphology of NiAl + 0.73 Re + 0.5Al_2O_3 powder after 4 h of milling in a planetary ball mill is shown in Fig. 2(b). Milling NiAl + 0.73Re + 0.5Al_2O_3 at 100 rpm resulted in defragmentation of the NiAl powder, but the sphericity of the particles was preserved. The comparison of particle size measured by laser diffraction (Malvern Mastersizer 3000) of raw NiAl powder, NiAl + 0.73Re + 0.5Al_2O_3 powder milled at 100 rpm (used as the starting powder in this paper), and NiAl + 0.73Re + 0.5Al_2O_3 powder milled at 200 rpm (used in (Ref 10)) is shown in Fig. 3.

The pure NiAl powder and the NiAl + 0.73Re + 0.5Al_2O_3 powder mixture were additively manufactured by using an ORLASC Creator 3D printer. In the first step, a parameter study was performed on the reference material (pure NiAl) for a range of parameters (Table 1) to calibrate the LPBF process.

Table 1 The parameters of the LPBF printing process used for pure NiAl

Parameter	Range
Laser power, W	65-250
Laser spot size, μm	80, 120
Hatching distance, μm	80-200
Layer height, μm	25
Energy input, J/mm^2	1.6-5

Table 2 The LPBF process parameters yielded stable parts

Parameter set no.	Laser power, W	Laser spot size, μm	Hatching distance, μm	Layer height, μm	Energy input, J/mm^2
1	250	80	80	25	4.5
2	**250**	**80**	**110**	**25**	**4.5**
3	250	120	140	25	3.24
4	250	120	170	25	4.5
5	250	120	200	25	4.5

The optimal set of parameters chosen to produce specimens is marked in bold

The optimal set of parameters was identified for pure NiAl (Table 2) and then used for the LPBF printing of the NiAl + 0.73Re + 0.5Al_2O_3 material.

Since the parameter set no. 2 in Table 2 resulted in the highest density of NiAl determined by the Archimedes method and the least amount of defects, it was selected for the fabrication of the specimens by the LPBF technique. Two types of specimens were printed by LPBF: (i) prismatic bars of dimensions 3.2 x 4.2 x 25 mm^3 (for mechanical tests), and (ii) disks of 48 mm in diameter and 5 mm in height. In the second stage of the material manufacturing process, the LPBF-printed 48 mm disks were consolidated in a hot press (HP, Thermal Technology LLC) in an argon atmosphere at a temperature of 1400 °C with a 10 °C/min heating rate, sintering pressure of 30 MPa, and a 60 min dwelling time.

Scanning electron microscopy (Zeiss Crossbeam 350) was used to characterize the microstructure of the materials. Prismatic specimens of 3 x 4 x 25 mm^3 were cut from 48 mm sinter disks using the Mitsubishi MV1200R wire cutter. Because of the strong influence of surface scratches and defects on the mechanical properties of NiAl (Ref 42), the prismatic specimens were ground and polished with a diamond suspension to 1 μm using a Presi Mecatech 334 polishing machine prior to mechanical testing. In addition to fracture toughness, which is the central property investigated in this study, the bending strength and hardness were also evaluated experimentally. The bending strength and fracture toughness (SEVNB probe) were measured in a four-point bending mode according to ISO 14704 (Ref 43) and ISO 23146:2012 (Ref 44) standards, respectively. At least five specimens were used in each test to obtain reliable average results. The hardness of the fabricated materials was evaluated using a Buehler Wilson VH1102 Micro Hardness Tester. The fracture mechanism during loading was examined in situ under SEM observation on the Kammrath-Weiss module on the same SEVNB specimens.

3. Results and Discussion

In what follows, a notation reflecting the manufacturing processes is introduced to distinguish between the fabricated materials. The (LPBF) label behind the chemical formula means that the material was produced by the laser powder bed fusion technique. In turn, the (LPBF + HP) label means that additional consolidation of the LPBF-printed material was applied using HP.

Table 3 Densities of the manufactured materials

Material	Measured density, g/cm^3	Theoretical density, g/cm^3	Relative density, %
NiAl (LPBF)	5.738	5.913	97.03
NiAl (LPBF + HP)	5.910	5.913	99.95
NiAl 0.73Re 0.5Al_2O_3 (LPBF)	5.943	6.010	98.89
NiAl 0.73Re 0.5Al_2O_3(LPBF + HP)	6.007	6.010	99.95

The densities of produced materials were evaluated according to the Archimedes method. The measured values are presented in Table 3. All the manufactured materials reveal high relative densities, especially those obtained by the combined (LPBF + HP) processing method.

Microstructural analysis by scanning electron microscopy (SEM) shows numerous cracks nucleated after the LPBF printing in both materials (Fig. 4a, c). The subsequent HP process applied to the LPBF samples has reduced the crack sizes or even made some cracks close, but structural defects can still be seen under the SEM (Fig. 4b, d).

The SEM/EDX analysis of the NiAl + 0.73Re + 0.5Al_2O_3 (LPBF) material shows that some aluminum oxide grains were detached from the surface during sample preparation. Figure 5(a) shows cavities left by the removed grains after the polishing process. This effect is caused by the low adhesion forces between the alumina and NiAl grains, which are directly related to the thermal stresses generated during the LPBF process. Some alumina grains are still present, and rhenium can be found as small grains of a few microns in size (Fig. 5b).

In contrast, the microstructure of the NiAl + 0.73Re + 0.5 Al_2O_3 (LPBF + HP) material shown in Fig. 6(a) is similar to the microstructure of NiAl + 0.73Re + 0.5Al_2O_3 prepared in (Ref 10) using HP sintering only. The ESB (Energy Selective Backscattered Electron) detector shows the distribution of aluminum oxide along the grain boundaries of NiAl (Fig. 6b). Besides the aluminum oxide powder added to NiAl by design, some in-situ created nanograins of aluminum oxide are detected as a result of the high-energy ball milling (Fig. 6a, b). After the hot pressing step, the interface between alumina and NiAl is much stronger due to the long exposure to high temperature and pressure. It should be added that rhenium grains in the NiAl + 0.73Re + 0.5Al_2O_3 LPBF + HP material do not form aggregates, similar to the NiAl + 0.73Re + 0.5Al_2O_3 HP material fabricated in Ref. (Ref 10).

The results of the mechanical tests are collectively shown in Table 4. It is clear from Table 4 that the mechanical properties of the materials produced by LPBF without post-processing consolidation by HP are poor. This is directly related to many thermally induced cracks during the LPBF process (see Fig. 4a, c). The basic requirements for the powder feedstock in all 3D printing techniques, such as spherical particle shape, high flow rate, and absence of satellites, were not fully achieved after the milling process of the NiAl + 0.73Re + 0.5Al_2O_3 powder (Fig. 2b), while the pure NiAl powder met these requirements much better (Fig. 2a). However, the main factor responsible for the low mechanical properties of the NiAl (LPBF) and NiAl + 0.73Re + 0.5Al_2O_3 (LPBF) materials was the thermal

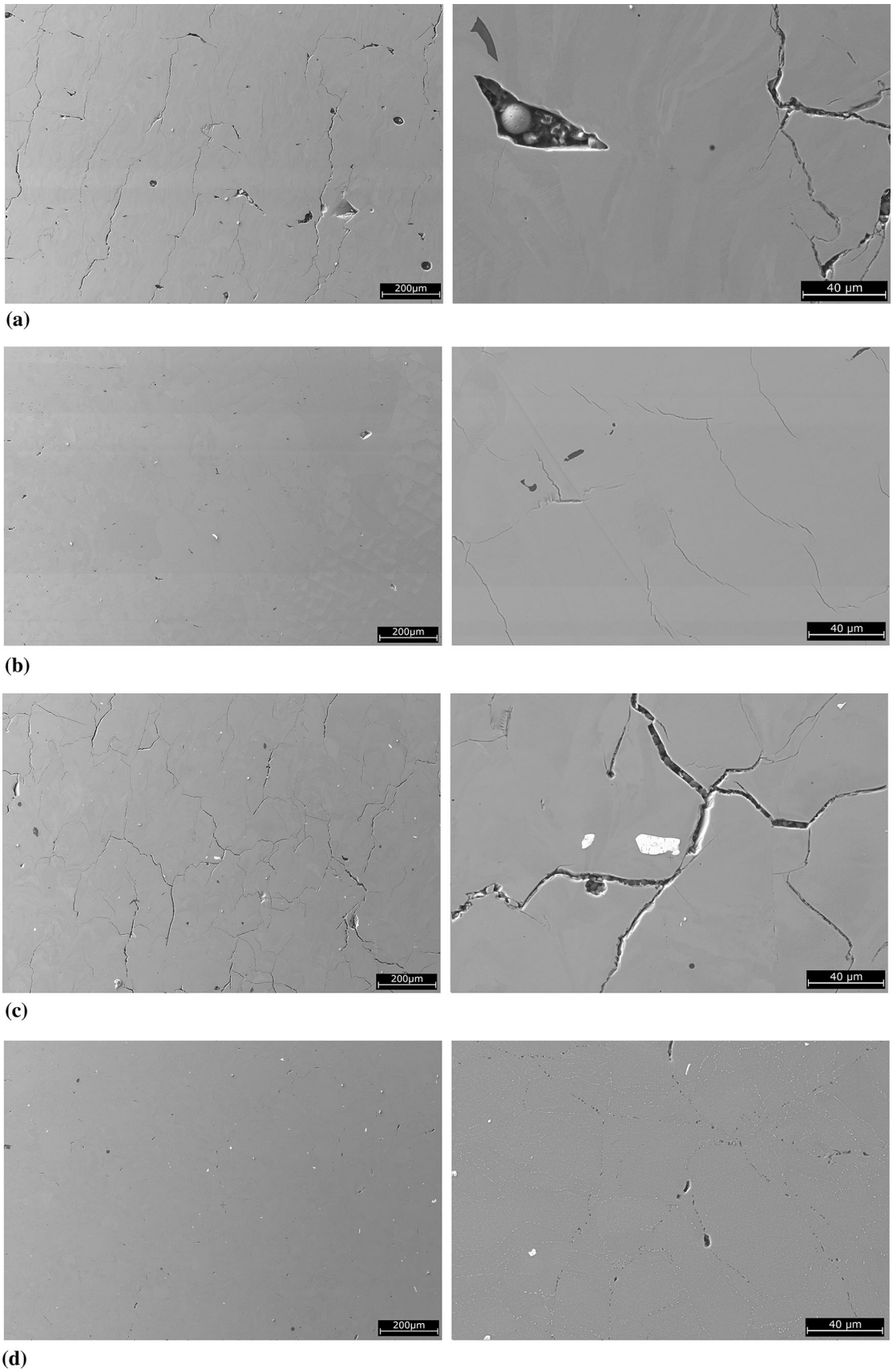

Fig. 4 SEM images (lower magnification on the left, higher on the right) of the microstructure of materials manufactured by LPBF: (a) NiAl, (c) NiAl + 0.73Re + 0.5Al_2O_3. Microstructure evolution in LPBF samples after consolidation by HP: (b) NiAl, (d) NiAl + 0.73Re + 0.5Al_2O_3.

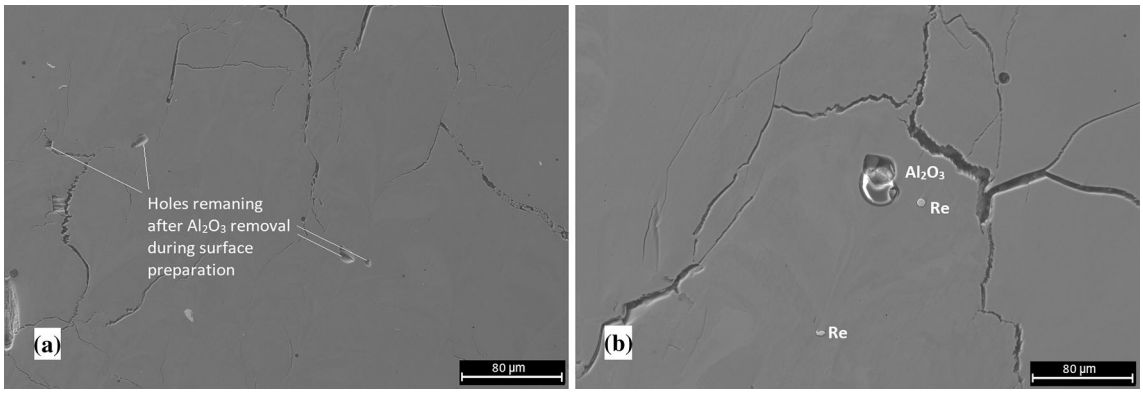

Fig. 5 SEM images of NiAl + 0.73Re + 0.5Al_2O_3 (LPBF) material: (a) cavities created by the extracted alumina grains during sample polishing; (b) some alumina still observed on the surface and rhenium identified as micrometric grains

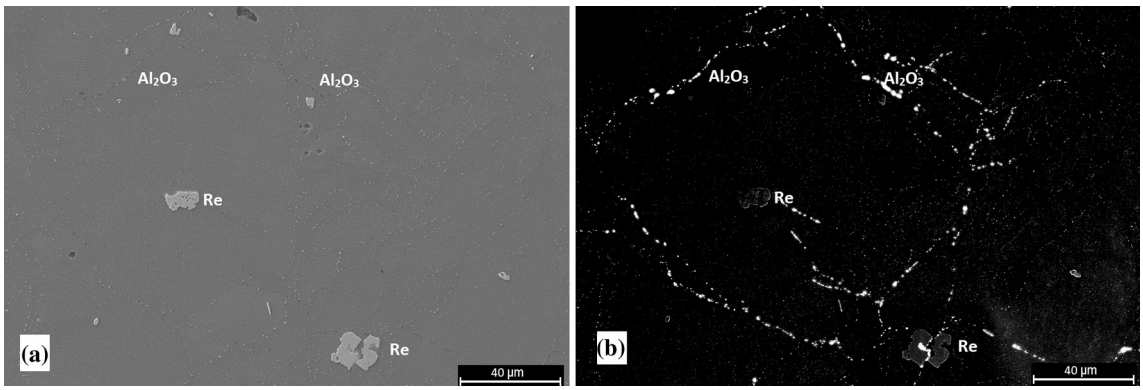

Fig. 6 SEM images of NiAl + 0.73Re + 0.5Al_2O_3 (LPBF + HP) material. SE detector image (a) and ESB detector image (b) indicate alumina and rhenium grains distributed in the NiAl matrix. The rhenium and alumina distributions are similar to those observed in NiAl + 0.73Re + 0.5Al_2O_3 material consolidated by singular HP (Ref 10).

Table 4 Mechanical properties of pure NiAl and NiAl + 0.73Re + 0.5Al_2O_3 samples produced by LPBF, HP, and LPBF + HP

Material	Bending strength, MPa	Fracture toughness, MPa $\sqrt{m}$	Hardness, HV1
NiAl (LPBF)	25.01 ± 4.28	2.83 ± 0.57	330.08 ± 17.4
NiAl (HP) (Ref 45)	345.6 ± 53.8	7.20 ± 0.40	n/a
NiAl (LPBF + HP)	347.74 ± 21.18	9.58 ± 0.77	331.00 ± 9.9
NiAl + 0.73Re + 0.5Al_2O_3 (LPBF)	25.90 ± 3.73	1.12 ± 0.16	340.94 ± 18.0
NiAl + 0.73Re + 0.5Al_2O_3 (HP) (Ref 10)	1065.1 ± 48.2	15.19 ± 2.51	n/a
NiAl + 0.73Re + 0.5Al_2O_3 (LPBF + HP)	311.39 ± 50.70	7.02 ± 1.17	341.98 ± 12.3

gradients generated during the LPBF printing, which led to crack nucleation (Fig. 4a, c).

When pressure-assisted sintering (HP) followed the LPBF process, the mechanical properties of the NiAl (LPBF + HP) and NiAl + 0.73Re + 0.5Al_2O_3 (LPBF + HP) materials were significantly improved compared to the NiAl (LPBF) and NiAl + 0.73Re + 0.5Al_2O_3 (LPBF) materials (Table 4). Surprisingly, the NiAl (LPBF + HP) showed superior properties to the NiAl + 0.73Re + 0.5Al_2O_3 (LPBF + HP). This is due to the fact that the NiAl + 0.73Re + 0.5Al_2O_3 powder mixture was not perfectly suited for the 3D printing process, while the NiAl powder was (see Fig. 2a, b).

The NiAl (LPBF + HP) material without the addition of alumina and rhenium exhibited a relatively high fracture toughness (K_{IC} = 9.58 MPa $\sqrt{m}$), which exceeded the fracture toughness of NiAl single crystals (Ref 46). The microhardness values of NiAl (LPBF) and NiAl (LPBF + HP) were almost equal (Table 4), as were the microhardness values of NiAl + 0.73Re + 0.5Al_2O_3 (LPBF) and NiAl + 0.73Re + 0.5Al_2O_3 (LPBF + HP). This means that the microhardness was not affected by the manufacturing process beacuse the NiAl grains were larger than the indentation trace.

The above described mechanical behavior of the obtained materials was directly reflected in the observed fracture mechanism investigated under SEM. In both materials produced by LPBF, reference NiAl and modified by rhenium and aluminum oxide additions, stable crack growth was observed during loading. Even in the presence of a sharp notch on the SEVNB specimen, the crack propagated mainly along the paths of thermally induced cracks, bypassing an artificially intro-

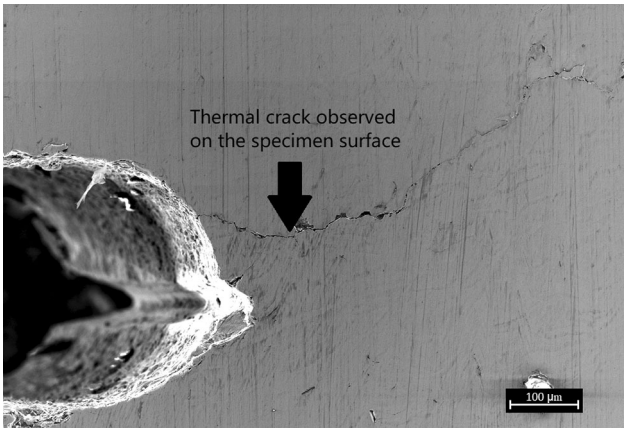

Fig. 7 Notch tip of NiAl + 0.73Re + 0.5Al_2O_3 LPBF specimen with a visible thermal crack on the specimen surface (initial state, 0N load)

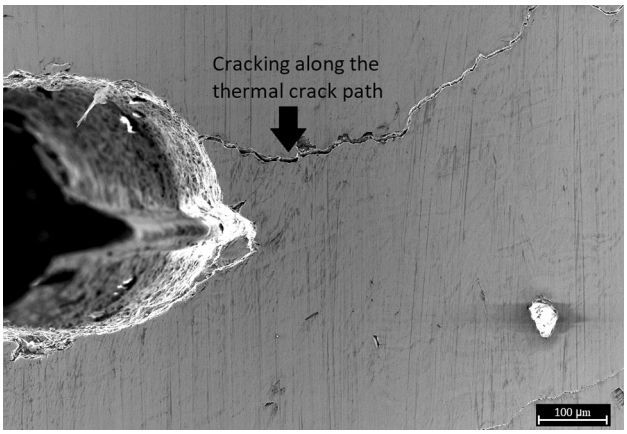

Fig. 8 Evolution of the thermal crack on the surface of NiAl + 0.73Re + 0.5Al_2O_3 LPBF notched specimen during loading in four-point bending SEVNB test

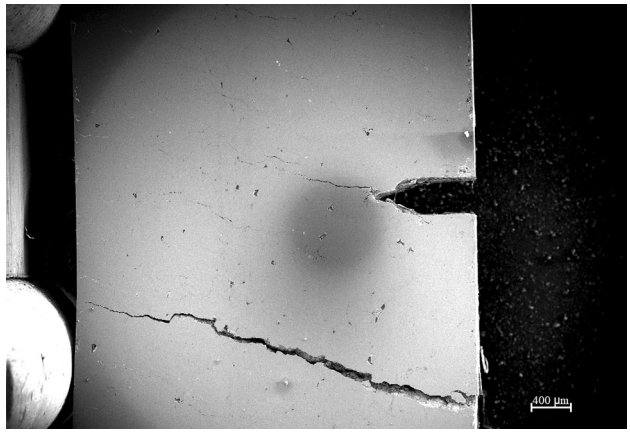

Fig. 9 In situ SEM image of NiAl notched specimen (LPBF) in four-point bending test showing fracture localized away from the notch zone

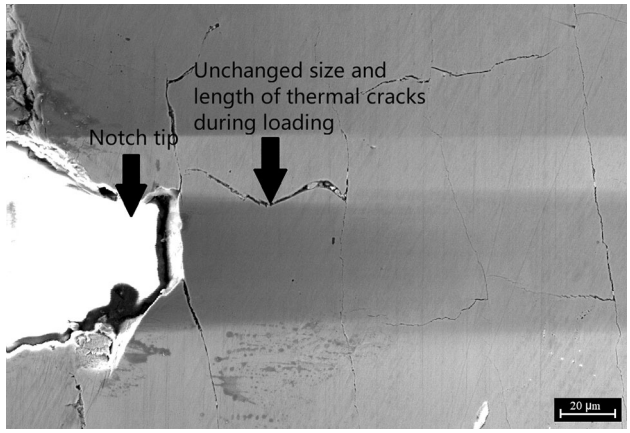

Fig. 10 SEM image of NiAl (LPBF + HP) notch tip at 200 N load level. No crack growth was observed up to 210 N.

duced notch tip (Fig. 7 and 8). The phenomenon of crack initiation and growth completely outside the notch area was also observed (Fig. 9).

As shown by the data in Table 4, the post-processing by HP resulted in significant increase in bending strength and fracture toughness of the NiAl and NiAl + 0.73Re + 0.5Al_2O_3 materials. The in situ bending tests performed under SEM indicate that the pre-crack tip at the notch is stable up to the maximum force. Due to the unstable crack propagation beyond the maximum load, the in situ SEM observation of the crack growth could not be performed. Figure 10 shows the area of the crack tip at a load level of 200 N, with the maximum applied force of 210 N.

Figure 11 shows the fracture surfaces after the SEVNB test in four-point bending mode. Typical river-type morphologies were observed in all of the manufactured materials. The fracture surface of NiAl (LPBF + HP) presented in Fig. 11b was the smoothest, indicating that the Ni-Al interface was not the weakest region of the material.

The irregular particle shapes and presence of satellites in the NiAl + 0.73Re + 0.5Al_2O_3 powder feedstock were the reasons for the poor mechanical properties of NiAl + 0.73Re + 0.5 Al_2O_3 samples produced by the LPBF process. Also, it is known that for aluminum alloys, which are prone to heat cracking, an addition of ceramic nanoparticles to the powder can prevent the formation of solidification cracks by acting as nucleation and grain refinement agents (Ref 47-49). The addition of rhenium and alumina to the NiAl powder feedstock did not improve the fracture toughness or the bending strength of the NiAl + 0.73Re + 0.5Al_2O_3 (LPBF) material compared to the NiAl + 0.73Re + 0.5Al_2O_3 (HP) material. It appears that the cracks in the LPBF material were primarily caused by the thermal stresses due to the rapid solidification of the melt pool in the process, rather than by solidification shrinkage. One measure to limit the thermally induced cracking could be a preheated plate or printing bed (Ref 28-31).

4. Conclusion

The laser powder bed fusion technique (LPBF) was adopted to produce bulk NiAl with the addition of rhenium and alumina to improve the room temperature fracture toughness of this intermetallic compound. The addition of Re and Al_2O_3 was justified by the promising results obtained previously in Ref. (Ref 9, 10) for the NiAl-Re-Al_2O_3 materials using the classical

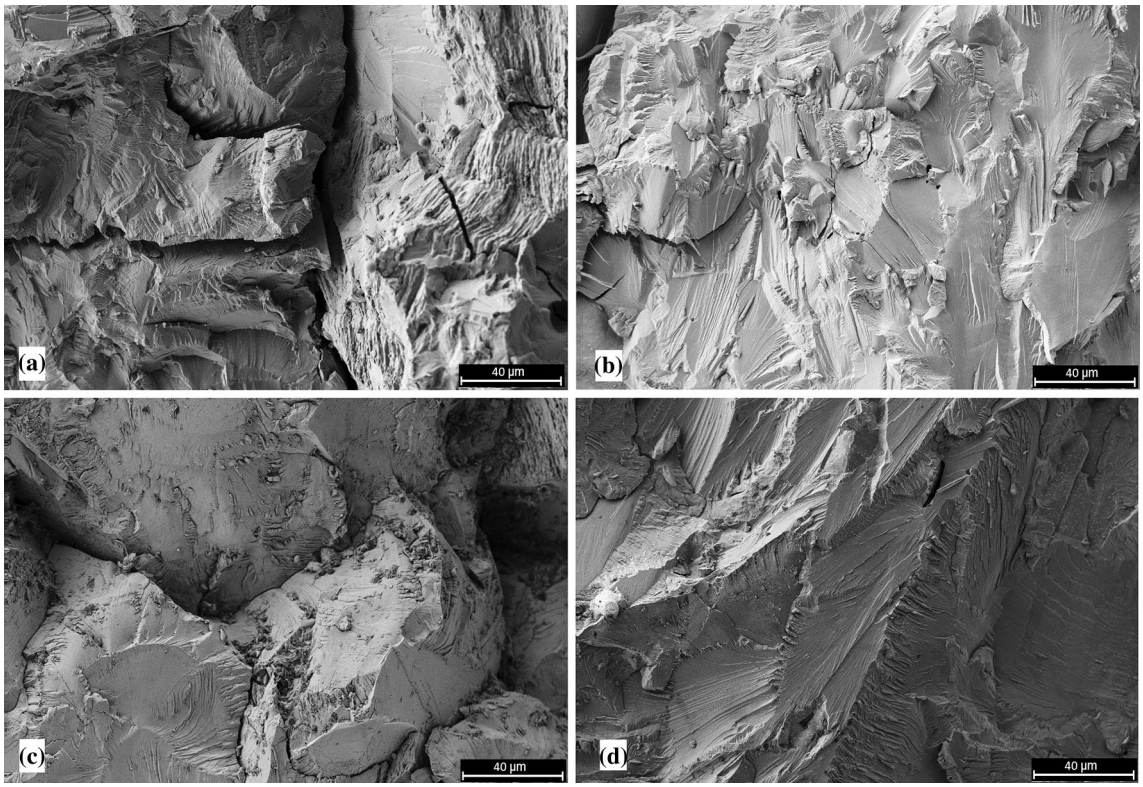

Fig. 11 Fracture surfaces of (a) NiAl (LPBF), (b) NiAl (LPBF + HP), (c) NiAl + 0.73Re + 0.5Al_2O_3 (LPBF), (d) NiAl + 0.73Re + 0.5Al_2O_3 (LPBF + HP) materials after the SEVNB test in four-point bending

powder metallurgy route (ball milling + hot pressing). A specific composition, namely NiAl + 0.73Re + 0.5Al_2O_3, was selected since it exhibited the highest mechanical properties when powder metallurgy was used as the processing technique (Ref 10). However, due to the cracks generated during the LPBF process, the fracture toughness and bending strength of the NiAl (LPBF) and NiAl + 0.73Re + 0.5Al_2O_3 (LPBF) materials turned out to be very low (Table 4). Post-processing of the LPBF-printed materials by hot pressing somewhat mitigated the thermal stress-induced cracking. As a consequence, an increase in K_{IC} and the bending strength of both NiAl (LPBF + HP) and NiAl + 0.73Re + 0.5Al_2O_3 (LPBF + HP) materials was noted. However, the fracture toughness of NiAl + 0.73Re + 0.5Al_2O_3 (LPBF + HP), K_{IC} = 7.02 MPa $\sqrt{m}$ was still much lower than K_{IC} = 15.19 MPa $\sqrt{m}$ for NiAl + 0.73Re + 0.5Al_2O_3 sintered by HP (Ref 10). As previously observed for NiAl + 0.73Re + 0.5Al_2O_3 produced by HP, the amount of 0.5 vol% of alumina acts similarly to the oxide dispersed strengthening mechanism, preventing grain growth during sintering. The homogeneous distribution of alumina grains at NiAl grain boundaries limits dislocation motion, thereby increasing the K_{IC} and bending strength. It should be noted that this effect is only valid for the well-defined amount of alumina addition. In the present work, however, the thermal cracking due to the LPBF process has a pronounced negative influence on the mechanical properties considered. In other words, the positive influence of admixture of fine aluminum oxide on mechanical properties is not observed when LPBF is used to produce this material.

Several factors responsible for this outcome can be pointed out. Firstly, the powder mixture NiAl + 0.73Re + 0.5Al_2O_3 used for the LPBF process was manufactured with different milling parameters than those used in the singular powder metallurgy route (Ref 10). It was proven in our previous research that the milling parameters can significantly influence the mechanical properties of NiAl (Ref 9, 10). In particular, when higher milling speeds were applied the ODS mechanism was observed. For LPBF, the well milled NiAl + 0.73Re + 0.5Al_2O_3 powder mixture prepared for singular HP sintering could not be used due to the limitations of the LPBF process. A preliminary trial was conducted, but the integrity of the LPBF material was poor due to the small particle size along with the high irregularity of milled particles. In addition, adverse structural effects that occurred during the LPBF process, such as thermally induced cracks, could not be remedied by applying hot pressing after the LPBF printing. Increasing the sintering temperature during hot pressing could reduce the material propensity to cracking. However, this could result in the liquefaction of the material if we get too close to the melting point. On the other hand, the HP step applied after the LPBF substantially improved the fracture toughness and the bending strength of the pure NiAl sample as shown in Table 4. Therefore, further research on processing bulk NiAl-Re-Al_2O_3 intermetallic materials by combining additive manufacturing and hot-pressing seems worth pursuing.

Acknowledgment

The preparation of NiAl and NiAl+073Re+0.5Al_2O_3 materials using the LPBF technique was performed at the Technische Universität Graz (Austria) during the research stay of Kamil Bochenek supported by the Research Fellowship (Call 2020) of the European Virtual Institute on Knowledge-based Multifunctional Materials (KMM-VIN AISBL).

References

1. A. Lasalmonie, Intermetallics: Why is it so Difficult to Introduce them in Gas Turbine Engines?, *Intermetallics*, 2006, **14**, p 1123–1129.
2. K. Bochenek and M. Basista, Advances in Processing of NiAl Intermetallic Alloys and Composites for High Temperature Aerospace Applications, *Prog. Aerosp. Sci.*, 2015, **79**, p 136–146.
3. R. Darolia, Ductility and Fracture Toughness Issues Related to Implementation of NiAl for Gas Turbine Applications, *Intermetallics*, 2000, **8**, p 1321–1327.
4. M.A. Awotunde, O.O. Ayodele, A.O. Adegbenjo, A.M. Okoro, M.B. Shongwe, and P.A. Olubambi, NiAl Intermetallic Composites — A Review of Processing Methods, Reinforcements and Mechanical Properties, *Int. J. Adv. Manuf. Technol.*, 2019, **104**, p 1733–1747.
5. J.T. Guo, C.Y. Cui, Y.X. Chen, D.X. Li, and H.Q. Ye, Microstructure, Interface and Mechanical Property of the DS NiAl/Cr(Mo, Hf) Composite, *Intermetallics*, 2001, **9**, p 287–297.
6. G. Frommeyer, R. Rablbauer, and H.J. Schäfer, Elastic Properties of B2-Ordered NiAl and NiAl-X (Cr, Mo, W) Alloys, *Intermetallics*, 2010, **18**, p 299–305.
7. J.-M. Yang, S.M. Jeng, K. Bain, and R.A. Amato, Microstructure and Mechanical Behavior of In-Situ Directional Solidified NiAl/Cr(Mo) Eutectic Composite, *Acta Mater.*, 1997, **45**, p 295–308.
8. D.R. Johnson, X.F. Chen, B.F. Oliver, R.D. Noebe, and J.D. Whittenberger, Directional Solidification and Mechanical Properties of NiAl-NiAlTa Alloys, *Intermetallics*, 1995, **3**, p 141–152.
9. K. Bochenek, W. Węglewski, J. Morgiel, and M. Basista, Influence of Rhenium Addition on Microstructure, Mechanical Properties and Oxidation Resistance of NiAl Obtained by Powder Metallurgy, *Mater. Sci. Eng. A*, 2018, **735**, p 121–130.
10. K. Bochenek, W. Węglewski, J. Morgiel, M. Maj, and M. Basista, Enhancement of Fracture Toughness of Hot-Pressed NiAl-Re Material by Aluminum Oxide Addition, *Mater. Sci. Eng. A*, 2020, **790**, 139670
11. J.L. Walter and H.E. Cline, The Effect of Solidification Rate on Structure and High-Temperature Strength of the Eutectic NiAl-Cr, *Metall. Mater. Trans.*, 1970, **1**, p 1221–1229.
12. F.E. Heredia, M.Y. He, G.E. Lucas, A.G. Evans, H.E. Dève, and D. Konitzer, The Fracture Resistance of Directionally Solidified Dual-Phase NiAl Reinforced with Refractory Metals, *Acta Metall. Mater.*, 1993, **41**(2), p 505–511.
13. G. Frommeyer and R. Rablbauer, High Temperature Materials Based on the Intermetallic Compound NiAl Reinforced by Refractory Metals for Advanced Energy Conversion Technologies, *Steel Res. Int.*, 2008, **79**, p 507–513.
14. G.K. Dey, Physical Metallurgy of Nickel Aluminides, *Sadhana - Acad. Proc. Eng. Sci.*, 2003, **28**, p 247–262.
15. D.B. Miracle, Deformation in NiAl Bicrystals, *Acta Metall. Mater.*, 1991, **39**, p 1457–1468.
16. T. Hong and A.J. Freeman, Effect of Antiphase Boundaries on the Electronic Structure and Bonding Character of Intermetallic Systems: NiAl, *Phys. Rev. B*, 1991, **43**, p 6446–6458.
17. J. Deges, A. Schneider, R. Fischer, and G. Frommeyer, APFIM Investigations on Quasi-Binary Hypoeutectic NiAl-Re Alloys, *Mater. Sci. Eng. A*, 2003, **353**, p 80–86.
18. O.M. Barabash, M.Y. Barabash, V.E. Oliker, and V.B. Sobolev, Effect of Rhenium on Formation of the Structure of Eutectic Alloys Based on β - NiAl + γ -Re, *Powder Metall. Metal Ceramics*, 2003, **42**, p 180–183.
19. R. Rablbauer, G. Frommeyer, and F. Stein, Determination of the Constitution of the Quasi-Binary Eutectic NiAl-Re System by DTA and Microstructural Investigations, *Mater. Sci. Eng. A*, 2003, **343**, p 301–307.
20. S.C. Ur and P. Nash, Secondary Recrystallization and High Temperature Compressive Properties of ODS MA NiAl, *Scr. Mater.*, 2002, **47**, p 405–409.
21. T. Volpp, E. Giiring, E. Arzt, and U.D.B. Mtinchen, Grain Size Determination and Limits to Hall-Petch Behavior in Nanocrystalline NiAl Powders, *Nanostruct. Mater.*, 1997, **8**, p 855–865.
22. H. Schleifenbaum, W. Meiners, K. Wissenbach, and C. Hinke, Individualized Production by Means of High Power Selective Laser Melting, *CIRP J. Manuf. Sci. Technol.*, 2010, **2**(3), p 161–169.
23. D. Buchbinder, H. Schleifenbaum, S. Heidrich, W. Meiners, and J. Bültmann, High Power Selective Laser Melting (HP SLM) of Aluminum Parts, *Phys. Procedia*, 2011, **12**, p 271–278.
24. Y. Liu, Z. Wu, W. Liu, and Y. Ma, Microstructure Evolution and Reaction Mechanism of Continuously Compositionally Ti/Al Intermetallic Graded Material Fabricated by Laser Powder Deposition, *J. Mater. Res. Technol.*, 2022, **20**, p 4173–4185.
25. Y.H. Zhou et al., Selective Laser Melting of Ti – 22Al – 25Nb Intermetallic: Significant Effects of Hatch Distance on Microstructural Features and Mechanical Properties, *J. Mater. Proc. Technol.*, 2020, **276**, p 116398.
26. M. Doubenskaia, A. Domashenkov, I. Smurov, and P. Petrovskiy, Study of Selective Laser Melting of intermetallic TiAl powder using integral analysis, *Int. J. Mach. Tools Manuf*, 2018, **129**(February), p 1–14.
27. H.P. Qu and H.M. Wang, Microstructure and Mechanical Properties of Laser Melting Deposited -TiAl Intermetallic Alloys, *Mater. Sci. Eng. A*, 2007, **466**, p 187–194.
28. Y. Kaplanskii, E.A. Levashov, A.V. Korotitskiy, P.A. Loginov, Z.A. Sentyurina, and A.B. Mazalov, In Fluence of Aging and HIP Treatment on the Structure and Properties of NiAl-Based Turbine Blades Manufactured by Laser Powder Bed Fusion, *Addit. Manuf.*, 2020, **31**, 100999
29. Y. Kaplanskii, A.A. Zaitsev, E.A. Levashov, P.A. Loginov, and Z.A. Sentyurina, NiAl Based Alloy Produced by HIP and SLM of Pre-Alloyed Spherical Powders. Evolution of the Structure and Mechanical Behavior at High Temperatures, *Mater. Sci. Eng. A*, 2018, **717**, p 48–59.
30. Y. Meng, J. Li, M. Gao, and X. Zeng, Microstructure Characteristics of Wire arc Additive Manufactured Ni-Al Intermetallic Compounds, *J. Manuf. Process.*, 2021, **68**, p 932–939.
31. D. Herzog, V. Seyda, E. Wycisk, and C. Emmelmann, Acta Materialia Additive Manufacturing of Metals, *Acta Mater.*, 2016, **117**, p 371–392.
32. G.L.M. Shunmugavel, A. Polishetty, M. Goldberg, and R. Singh, A Comparative Study of Mechanical Properties and Machinability of Wrought and Additive Manufactured (Selective Laser Melting) Titanium Alloy - Ti-6Al-4V, *Rapid Prototyp. J.*, 2023, **23**(6), p 1051–1056.
33. P.M.K. Bochenek, R.S.M. Koralnik, K.J.M. Wieczorek, and Z.P.J. Mizera, Comparison of Mechanical Properties and Structure of Haynes 282 Consolidated Via Two Different Powder Metallurgy Methods: : Laser Powder Bed Fusion and Hot Pressing, *Arch. Civ. Mech. Eng.*, 2023, **23**(2), p 130.
34. P.A. Colegrove, J. Donoghue, F. Martina, J. Gu, P. Prangnell, and J. Hönnige, Application of Bulk Deformation Methods for Microstructural and Material Property Improvement and Residual Stress and Distortion Control in Additively Manufactured Components, *Scr. Mater.*, 2017, **135**, p 111–118.
35. S. Imam et al., Post Fabrication Thermomechanical Processing of Additive Manufactured Metals: : A Review, *J. Manuf. Process.*, 2022, **73**, p 757–790.
36. F. Meiners et al., New Hybrid Manufacturing Routes Combining Forging and Additive Manufacturing to Efficiently Produce High Performance Components from Ti-6Al-4V, *Procedia Manuf.*, 2020, **47**, p 261–267.
37. M. Merklein, D. Junker, A. Schaub, F. Neubauer. Hybrid additive manufacturing technologies - An analysis regarding potentials and applications. In: *Physics Procedia 9th International Conference of Photonic Technologies - Lane 2016*, 2016, vol. 83, pp. 549–559
38. G. Manogharan, R.A. Wysk, and O.L.A. Harrysson, Additive Manufacturing-Integrated Hybrid Manufacturing and Subtractive Processes:

Economic Model and Analysis, *Procedia Eng.*, 2016, **29**(5), p 473–488.
39. D. Strong, M. Kay, B. Conner, T. Wake, and G. Manogharan, Hybrid Manufacturing – Integrating Traditional Manufacturers with Additive Manufacturing (AM) Supply Chain, *Add. Manuf.*, 2018, **21**, p 159–173.
40. M. Khomutov, P. Potapkin, V. Cheverikin, P. Petrovskiy, A. Travyanov, and I. Logachev, Intermetallics Effect of Hot Isostatic Pressing on Structure and Properties of Intermetallic NiAl – Cr – Mo Alloy Produced by Selective Laser Melting, *Intermetallics*, 2020, **120**, p 106766.
41. T. Voisin, J.P. Monchoux, L. Durand, N. Karnatak, M. Thomas, and A. Couret, An Innovative Way to Produce γ-TiAl Blades: Spark Plasma Sintering, *Adv. Eng. Mater.*, 2015, **17**, p 1408–1413.
42. R. Darolia and W.S. Walston, Effect of Specimen Surface Preparation on Room Temperature Tensile Ductility of an Fe-Containing NiAl Single Crystal Alloy, *Intermetallics*, 1996, **4**, p 505–516.
43. "ISO 14704, Fine ceramics (advanced ceramics, advanced technical ceramics) — Test method for flexural strength of monolithic ceramics at room temperature," 2016
44. "ISO 23146 Advanced Technical Ceramics - Test methods for fracture toughness of monolithic ceramics - Single-edge V-notch beam (SEVNB) method," 2015
45. D. Kaliński, M. Chmielewski, K. Pietrzak, and K. Choręgiewicz, An Influence of Mechanical Mixing and Hot-Pressing on Properties of NiAl/Al2O3 Composite, *Arch. Metall. Mater.*, 2012, **57**, p 695–702.
46. R.D. Noebe, A. Misra, and R. Gibala, Plastic Flow and Fracture of B2 NiAl-Based Intermetallic Alloys Containing a Ductile Second Phase, *ISIJ Int.*, 1991, **31**, p 1172–1185.
47. Y. Otani and S. Sasaki, Effects of the Addition of Silicon to 7075 Aluminum Alloy on Microstructure, Mechanical Properties, and Selective Laser Melting Processability, *Mater. Sci. Eng. A*, 2020, **777**, p 139079.
48. B. Huang, Y. Liu, Z. Zhou, W. Cheng, and X. Liu, Selective Laser Melting of 7075 Aluminum Alloy Inoculated by Al–Ti–B: Grain Refinement and Superior Mechanical Properties, *Vacuum*, 2022, **200**, p 111030.
49. J.H. Martin, B.D. Yahata, J.M. Hundley, J.A. Mayer, T.A. Schaedler, and T.M. Pollock, 3D Printing of High-Strength Aluminium Alloys, *Nature*, 2017, **549**(7672), p 365–369.